

Boundary Conditions for Compressible Unsteady Flows.

F. Nicoud and T. Poinso

CERFACS - 42, Av. Gaspard Coriolis, 31057 Toulouse, FRANCE
E-mail: nicoud@cerfacs.fr or poinso@cerfacs.fr

Abstract

Several characteristics-based boundary conditions for the unsteady Euler equations are written in a unified framework to underline their common features as well as their differences. Their extension to the Navier-Stokes equations is then discussed. Various model test cases are used to illustrate the sensitivity of unsteady flows to the boundary conditions. Finally, more complex computations involving flow instabilities are discussed from the perspective of the boundary treatment.

1 Introduction

Over the last decades, algorithmic improvements and increase of computational power have led to solvers with higher levels of accuracy. Accurate computation of unsteady compressible flow is needed in e.g. aeroacoustics, self-sustained instabilities and combustion instabilities. Typical approaches are Direct Numerical Simulation (DNS), Large Eddy Simulation (LES), Reynolds-averaged Navier-Stokes equations, or even simpler models like the Euler equations. A major subject for industrial computation has been, and still is, steady state flow. It is important to converge rapidly to steady state, and it has been recognized that dissipative schemes help, but affect the accuracy. Unsteady computations have to reproduce wave propagation, and dissipative schemes are out of the question from the start. With more accurate schemes, higher demands are put on the boundary conditions which must permit waves to leave the domain without unwanted reflections. Some studies indicate that reflections may be of numerical origin.

Practical applications need various inflow and outflow boundary conditions like non-reflecting inlet or outlet, unsteady inlet with fluctuating velocity fields, as well as wall conditions. These conditions should meet the following criteria:

- The right number of constraints has to be imposed at a given boundary to ensure well-posedness. This number can be derived analytically [1, 2, 3, 4].
- The physics of the problem has to be properly translated into the wave/boundary interactions. For example, with a pressure imposed outlet, an acoustic wave leaving the domain should be transformed into an ingoing one of the same amplitude.
- A numerical implementation of the mathematical and physical statements has to be chosen so as to minimize the numerical perturbations generated at the boundaries. There is clear experimental evidence that backward propagating acoustic waves may trigger an hydrodynamic instability of the Kelvin-Helmholtz type [5]. If the acoustic wave comes from any physical sound generation process, this interaction leads to a feedback instability. However, if the acoustic wave is induced by an improper boundary treatment, the obtained feedback loop has no physical meaning [6, 7].
- The properties of the initial flowfield should become unimportant after a characteristic time of the problem has been computed. This requirement seems obvious for any unsteady or

steady computation, but may not be met by certain advanced boundary conditions.

Different boundary condition treatments based on the characteristic approach have been proposed in the literature [8, 9, 10, 11], which satisfy in various degrees the above requirements. Several authors focused essentially on the best way to write a non-reflecting boundary condition for the Euler equations [12, 13, 14, 15] (see Givoli [16] for a complete review). It is now commonly accepted [17, 18, 19] that a perfect formulation is not reachable for the non-linear case and it has been found necessary to add non physical exit zones onto the computation domain. This paper is not concerned with these zonal formulations because of their lack of flexibility and because the additional cost may be high [17]. Its objective is to clarify the common points of some characteristic boundary conditions found in literature, as well as the way they differ from an analytical point of view. We also show on simple unsteady test cases how these formal differences change the results. Section 2 presents the general ideas behind the characteristic approach for the boundary conditions. The particular case of prescribing a non-reflecting condition is discussed in Section 3 and a general procedure to account for the viscous terms is presented in Section 4. Section 5 shows to what extent the quality of the results for unsteady computations is improved or damaged by the choice of the boundary condition.

2 The Characteristic Boundary Conditions

For hyperbolic equations, most advanced boundary treatments make use of the characteristic approach, which is described in many basic articles or textbooks [11]. Characteristic boundary conditions are based on distinguishing ingoing and outgoing waves at the boundary of the domain. Information carried by outgoing waves is left untouched, while the boundary condition must supply information corresponding to the ingoing waves. This can take the form of e.g. prescribing the strength of ingoing waves, or extrapolating characteristic variables, or Riemann invariants.

The time dependent Euler equations are hyperbolic, and can be reformulated in a set of characteristic advection equations. Let us consider the 3D Euler equations in quasi-linear form:

$$\frac{\partial \mathbf{V}}{\partial t} + \mathbf{A} \frac{\partial \mathbf{V}}{\partial x} + \mathbf{B} \frac{\partial \mathbf{V}}{\partial y} + \mathbf{C} \frac{\partial \mathbf{V}}{\partial z} = \mathbf{0}. \quad (1)$$

In this equation, $\mathbf{V} = (\rho, u, v, w, P)^T$ is the vector of the primitive

variables and the matrices \mathbf{A} , \mathbf{B} and \mathbf{C} are defined as:

$$\mathbf{A} = \begin{bmatrix} u & \rho & \cdot & \cdot & \cdot \\ \cdot & u & \cdot & \cdot & 1/\rho \\ \cdot & \cdot & u & \cdot & \cdot \\ \cdot & \cdot & \cdot & u & \cdot \\ \cdot & \gamma P & \cdot & \cdot & u \end{bmatrix} \quad \mathbf{B} = \begin{bmatrix} v & \cdot & \rho & \cdot & \cdot \\ \cdot & v & \cdot & \cdot & \cdot \\ \cdot & \cdot & v & \cdot & 1/\rho \\ \cdot & \cdot & \cdot & v & \cdot \\ \cdot & \cdot & \gamma P & \cdot & v \end{bmatrix} \quad \mathbf{C} = \begin{bmatrix} w & \cdot & \cdot & \rho & \cdot \\ \cdot & w & \cdot & \cdot & \cdot \\ \cdot & \cdot & w & \cdot & \cdot \\ \cdot & \cdot & \cdot & w & 1/\rho \\ \cdot & \cdot & \cdot & \gamma P & w \end{bmatrix}, \quad (2)$$

where γ , ρ , $\vec{v} = (u, v, w)^T$ and P represent the isentropic coefficient, the density, the velocity vector and the static pressure respectively. Each of the matrices \mathbf{A} , \mathbf{B} and \mathbf{C} has its own complete set of real eigenvalues and of right and left eigenvectors, which differ from one matrix to the other. The matrix \mathbf{E}_n defined as $\mathbf{A}n_x + \mathbf{B}n_y + \mathbf{C}n_z$ is introduced, where \vec{n} is an arbitrary unit vector. The eigenvalues matrix obtained by diagonalizing \mathbf{E}_n reads as:

$$\mathbf{\Lambda}_n = \mathbf{L}_n \mathbf{E}_n \mathbf{L}_n^{-1} = \text{diag}(\lambda_n^1, \lambda_n^2, \lambda_n^3, \lambda_n^4, \lambda_n^5) = \text{diag}(u_n, u_n, u_n, u_n + c, u_n - c), \quad (3)$$

where $u_n = \vec{u} \cdot \vec{n}$ and c is the speed of sound. The matrices with left (resp. right) eigenvectors as rows (resp. columns) \mathbf{L}_n and \mathbf{L}_n^{-1} are given by

$$\mathbf{L}_n = \begin{pmatrix} 1 & 0 & 0 & 0 & -1/c^2 \\ 0 & s_{1x} & s_{1y} & s_{1z} & 0 \\ 0 & s_{2x} & s_{2y} & s_{2z} & 0 \\ 0 & n_x & n_y & n_z & 1/\rho c \\ 0 & -n_x & -n_y & -n_z & 1/\rho c \end{pmatrix}, \quad \text{and } \mathbf{R}_n = \mathbf{L}_n^{-1} = \begin{pmatrix} 1 & 0 & 0 & \rho/2c & \rho/2c \\ 0 & s_{1x} & s_{2x} & n_x/2 & -n_x/2 \\ 0 & s_{1y} & s_{2y} & n_y/2 & -n_y/2 \\ 0 & s_{1z} & s_{2z} & n_z/2 & -n_z/2 \\ 0 & 0 & 0 & \rho c/2 & \rho c/2 \end{pmatrix}. \quad (4)$$

They relate variations of the characteristic variables \mathbf{W}_n to the variations of the primitive vector \mathbf{V} by:

$$\delta \mathbf{W}_n = \mathbf{L}_n \delta \mathbf{V} \quad \delta \mathbf{V} = \mathbf{L}_n^{-1} \delta \mathbf{W}_n, \quad (5)$$

or :

$$\delta \mathbf{W}_n = \begin{bmatrix} \delta W_n^1 \\ \delta W_n^2 \\ \delta W_n^3 \\ \delta W_n^4 \\ \delta W_n^5 \end{bmatrix} = \begin{bmatrix} \delta \rho - \frac{1}{c^2} \delta P \\ \vec{s}_1 \cdot \delta \vec{u} \\ \vec{s}_2 \cdot \delta \vec{u} \\ + \vec{n} \cdot \delta \vec{u} + \frac{1}{\rho c} \delta P \\ - \vec{n} \cdot \delta \vec{u} + \frac{1}{\rho c} \delta P \end{bmatrix} \quad (6)$$

and

$$\delta \mathbf{V}_n = \begin{bmatrix} \delta \rho \\ \delta u \\ \delta v \\ \delta w \\ \delta P \end{bmatrix} = \begin{bmatrix} \delta W_n^1 + \frac{\rho}{2c}(\delta W_n^4 + \delta W_n^5) \\ s_{1x}\delta W_n^2 + s_{2x}\delta W_n^3 + \frac{n_x}{2}(\delta W_n^4 - \delta W_n^5) \\ s_{1y}\delta W_n^2 + s_{2y}\delta W_n^3 + \frac{n_y}{2}(\delta W_n^4 - \delta W_n^5) \\ s_{1z}\delta W_n^2 + s_{2z}\delta W_n^3 + \frac{n_z}{2}(\delta W_n^4 - \delta W_n^5) \\ \frac{\rho c}{2}(\delta W_n^4 + \delta W_n^5) \end{bmatrix}. \quad (7)$$

Unit vectors \vec{s}_1 and \vec{s}_2 are such that they form with \vec{n} an orthonormal basis $(\vec{n}, \vec{s}_1, \vec{s}_2)$. Note that for each unit vector \vec{n} , a different set of characteristic variables is obtained. Also the choice of right and left eigenvectors influences the scaling of the characteristic variables. Every author has his/her own preferences, but this is not important for the remainder of this paper. The first characteristic variation is proportional to entropy variations, the second and third are related to variations in shear velocity, and the last two represent acoustic disturbances.

The five characteristic variables satisfy a set of convection equations, the compatibility equations, with the speed of propagation given by Eq. (3) and with source terms related to pressure and velocity variations in the (\vec{s}_1, \vec{s}_2) -plane. These equations are obtained by premultiplying Eq. (1) with \mathbf{L}_n :

$$\begin{aligned} \frac{\partial W_n^1}{\partial t} + \vec{u} \cdot \vec{\nabla} W_n^1 &= 0, \\ \frac{\partial W_n^2}{\partial t} + \vec{u} \cdot \vec{\nabla} W_n^2 + \frac{1}{2} c \vec{s}_1 \cdot (\vec{\nabla} W_n^4 + \vec{\nabla} W_n^5) &= 0, \\ \frac{\partial W_n^3}{\partial t} + \vec{u} \cdot \vec{\nabla} W_n^3 + \frac{1}{2} c \vec{s}_2 \cdot (\vec{\nabla} W_n^4 + \vec{\nabla} W_n^5) &= 0, \\ \frac{\partial W_n^4}{\partial t} + (\vec{u} + c\vec{n}) \cdot \vec{\nabla} W_n^4 + c (\vec{s}_1 \cdot \vec{\nabla} W_n^2 + \vec{s}_2 \cdot \vec{\nabla} W_n^3) &= 0, \\ \frac{\partial W_n^5}{\partial t} + (\vec{u} - c\vec{n}) \cdot \vec{\nabla} W_n^5 + c (\vec{s}_1 \cdot \vec{\nabla} W_n^2 + \vec{s}_2 \cdot \vec{\nabla} W_n^3) &= 0. \end{aligned} \quad (8)$$

In general, these equations are decoupled only in 1D, where the second and third line vanish, with $\vec{s}_1 = \vec{s}_2 = \vec{0}$. In the case of the Navier-Stokes equations, additional source terms appear.

For boundary conditions, \vec{n} is chosen normal to the considered boundary, either inward or outward. In the following, we take the normal outward, which means that negative speed represents information

convected into the computational domain. Positive speeds correspond to information leaving the domain, independent of the physical boundary condition. However, the decomposition of the Euler equations into a set of waves with \vec{n} normal to the boundary is a crude and sometimes inadequate assumption [20].

The ingoing information depends on the physical boundary condition, the numerical evaluation of outgoing waves, the truncation error in the boundary approximation chosen and the way relevant boundary variables are updated. Several methods can be used, which can be classified in different ways. Without being complete, we distinguish:

- Extrapolation methods. Space, time or space-time extrapolation of the conservative/primitive [21, 22] or characteristic [23] variables are used. This includes e.g. a symmetry condition by annihilating normal velocity, or a wall boundary condition which sets the speed to zero for Navier Stokes equations. Characteristic extrapolation includes the use of Riemann invariants which we will discuss and test here (see sections 3.3 and 3.4.1).
- Application of boundary conditions at the level of the partial differential equations. This can be done in the compatibility relations [11], or in the equations of motion [10], with a one-sided discretization. This latter technique is more appropriate for the Navier-Stokes equations, when the boundary conditions have to be separated from the viscous terms. In this paper, we will focus on this category, which has in common that the boundary conditions act on *variations*, rather than on the variables themselves. It means that the strength of incoming waves is calculated as a function of the physical boundary conditions imposed and the strength of the outgoing waves.

Applying an Euler explicit time discretization to Eq. (1), the update of primitive variables can be written as:

$$\Delta \mathbf{V} = \mathbf{V}^{n+1} - \mathbf{V}^n = -\Delta t \mathcal{R} = -\Delta t \left[\mathbf{A} \frac{\partial \mathbf{V}}{\partial x} + \mathbf{B} \frac{\partial \mathbf{V}}{\partial y} + \mathbf{C} \frac{\partial \mathbf{V}}{\partial z} \right] \quad (9)$$

For a given boundary with normal \vec{n} , the full residual \mathcal{R} in Eq. (9) can be split into a normal part \mathcal{R}_n (involving only normal derivatives) and a tangential part \mathcal{R}_s (involving only derivatives along \vec{s}_1 and \vec{s}_2) so that $\mathcal{R} = \mathcal{R}_n + \mathcal{R}_s$. E.g., if $\vec{n} = (1, 0, 0)^t$, that is \vec{n} aligned with the x -axis, $\mathcal{R}_n = \mathbf{A} \partial \mathbf{V} / \partial x$ and $\mathcal{R}_s = \mathbf{B} \partial \mathbf{V} / \partial y + \mathbf{C} \partial \mathbf{V} / \partial z$.

Let us call \mathbf{V}^n the boundary value at time level n , $\delta \mathbf{V}^P$ the predicted boundary update due to the interior scheme, before application of the boundary conditions, $\delta \mathbf{V}_w^P$ the part of $\delta \mathbf{V}^P$ to which the boundary conditions will be applied, and $\delta \mathbf{V}^U = \delta \mathbf{V}^P - \delta \mathbf{V}_w^P$ the part of the

boundary update which is not affected by the characteristic boundary conditions. As an example, in methods which identify waves only using terms normal to the boundary, $\delta\mathbf{V}_w^P$ is the predicted value of $-\Delta t\mathcal{R}_n$ and $\delta\mathbf{V}^U$ is equal to $-\Delta t\left[\mathbf{B}\frac{\partial\mathbf{V}}{\partial y} + \mathbf{C}\frac{\partial\mathbf{V}}{\partial z}\right]$. Note that $\delta\mathbf{V}^U$ could also contain other contributions like the diffusive terms in the case of the Navier-Stokes equations or the heat release for combustion. The boundary conditions are then applied as follows:

1. Decide the part $\delta\mathbf{V}_w^P$ of the residual to which the boundary conditions are going to be applied to. If it is the full residual, then $\delta\mathbf{V}^U = 0$.
2. Using Eq. (6), decompose $\delta\mathbf{V}_w^P$, into characteristic variations $\delta W_n^{in,P}$ and δW_n^{out} due to ingoing and outgoing waves, with corresponding primitive variations $\delta\mathbf{V}_w^{in,P}$ and $\delta\mathbf{V}_w^{out}$.
3. Modify the amplitude of the incoming wave(s) $\delta W_n^{in,P}$ corresponding to the physical requirements at the boundary. This gives corrected amplitudes, $\delta W_n^{in,C}$. Keep the outgoing waves δW_n^{out} or $\delta\mathbf{V}_w^{out}$ as they are. As an example, consider a pressure imposed subsonic outlet, $\delta P = 0$. The characteristic speeds u_n and $u_n + c$ are positive, and the only wave to be affected by the boundary condition is the ingoing acoustic with speed $u_n - c$. Eq. (7) states that $\delta P = \delta W_n^4 + \delta W_n^5$, which gives $\delta W_n^{5,C} = -\delta W_n^4$.
4. Combine the waves $\delta W_n^{in,C}$ and δW_n^{out} , and transform back to primitive variables using \mathbf{L}_n^{-1} , Eq. (7). This gives $\delta\mathbf{V}_w^C$. The boundary point is then updated according to

$$\mathbf{V}^{n+1} = \mathbf{V}^n + \delta\mathbf{V}^U + \delta\mathbf{V}_w^C = \mathbf{V}^n + \delta\mathbf{V}^U + \delta\mathbf{V}^{in,C} + \delta\mathbf{V}^{out}$$

The decomposition of the Euler equations into a set of waves traveling normally to the boundary provides us with a theoretical basis to derive proper boundary condition treatments. However the theory says nothing on the best choice for defining the part of the update related to the waves ($\delta\mathbf{V}_w^P$). In what we call the *full residual* approach [24] the boundary conditions are applied to the full residual, viz. $\delta\mathbf{V}^P = -\Delta t\mathcal{R} = \delta\mathbf{V}_w^P$. In this case the update becomes $\mathbf{V}^{n+1} = \mathbf{V}^n + \delta\mathbf{V}_w^C = \mathbf{V}^n + \delta\mathbf{V}^{in,C} + \delta\mathbf{V}^{out}$. An alternative is the *normal* approach where $\delta\mathbf{V}_w^P = -\Delta t\mathcal{R}_n$. It has been proposed by Thompson [9] for the non-reflecting condition and by Poinsot and Lele [10] as a basis of a general procedure to derive boundary conditions for the Navier-Stokes equations. A part of the residual ($\delta\mathbf{V}^U$) is not touched by the boundary conditions, and therefore, an additional non-characteristic correction is needed. The effect of the definition of the wave strength is discussed in more details in Section 3 for the particular case of a non-reflecting boundary condition (see also [25]).

3 Non-Reflecting Conditions

3.1 Non-reflecting boundary conditions

It is straightforward to derive the strength of the incoming waves for physical boundary conditions like an outlet where pressure is imposed. Likewise, an inlet with total pressure and temperature and the flow angles, or total temperature and mass flux poses no problem. It is more complicated to design a non-reflecting boundary condition [25].

The simplest form of this condition is to set the strength of the incoming wave to zero. In 2D, with W^4 the ingoing characteristic for a subsonic outlet, the *full residual* approach gives [8, 13, 26, 24]:

$$\frac{\partial W^4}{\partial t} = 0 \quad (10)$$

whereas the *normal* approach leads to [9, 10]:

$$(u_n - c) \frac{\partial W^4}{\partial n} = 0 \quad (11)$$

Hirsch[11] argues that non-reflecting condition has to be applied to the advection terms of the bicharacteristic equations:

$$(u_n - c) \frac{\partial W^4}{\partial n} + u_s \frac{\partial W^4}{\partial s} = 0. \quad (12)$$

A more elaborate analysis is performed by Engquist and Majda [2], and translated for practical implementation by Giles[12]. The analysis for the linearized Euler equations is based on a Fourier decomposition of the solution at the boundary, that is decomposition of plane waves in arbitrary directions. Now, the strength of each ingoing Fourier component is set to zero, and consequently, the ingoing waves in the space-time domain are finite. This introduces a dependency of the incoming characteristic on the tangential derivatives at the boundary. For one-dimensional flow, Eq. (10) is recovered. Here we consider the approximate, two-dimensional unsteady formulation [12], which for a 2D outlet gives:

$$\frac{\partial W^4}{\partial t} = -u_n \frac{\partial W^4}{\partial s} - u_s \frac{\partial W^4}{\partial s}, \quad (13)$$

where u_n and u_s are the normal and tangential velocity at the boundary, and $\partial/\partial s$ denotes the tangential derivative.

Eq. (10), (11), (12) and (13) are all non-reflecting boundary conditions based on characteristic analysis. They do not produce the same

results however. This may be explained by formulating all of them in the same framework: indeed, any (non-reflecting) boundary condition can be written either in terms of time derivatives (*temporal form*) or in terms of normal derivative (*spatial form*). These two forms are linked by the compatibility relations, Eq. (8), and imposing a boundary condition on the time derivative can be translated into a condition on the normal derivative and vice versa. An overview of the presented conditions written in their two equivalent forms (*temporal* and *spatial*) is given in table 1. A key reference is used to name each boundary condition. The conversion between the two forms may be obtained with the 2D version of the compatibility relations which for the ingoing characteristic reduces to:

$$\frac{\partial W^4}{\partial t} + (u_n - c) \frac{\partial W^4}{\partial n} + u_s \frac{\partial W^4}{\partial s} + c \frac{\partial W^2}{\partial s} = 0. \quad (14)$$

Name	<i>temporal form</i>	<i>spatial form</i>
Thompson [24]	$\frac{\partial W^4}{\partial t} = 0$ Eq. (10)	$\frac{\partial W^4}{\partial n} = -\frac{1}{u_n - c} \left\{ u_s \frac{\partial W^4}{\partial s} + c \frac{\partial W^2}{\partial s} \right\}$
Poinsot [10]	$\frac{\partial W^4}{\partial t} = -\left\{ u_s \frac{\partial W^4}{\partial s} + c \frac{\partial W^2}{\partial s} \right\}$	$\frac{\partial W^4}{\partial n} = 0$ Eq. (11)
Hirsh [11]	$\frac{\partial W^4}{\partial t} = -c \frac{\partial W^2}{\partial s}$	$\frac{\partial W^4}{\partial n} = -\frac{u_s}{(u_n - c)} \frac{\partial W^4}{\partial s}$ Eq. (12)
Giles [12]	$\frac{\partial W^4}{\partial t} = -u_n \frac{\partial W^2}{\partial s} - u_s \frac{\partial W^4}{\partial s}$ Eq. (13)	$\frac{\partial W^4}{\partial n} = \frac{\partial W^2}{\partial s}$

Table 1: *Correspondance between the temporal and the spatial form for some non-reflecting boundary conditions. 2D case.*

This table provides a way to formally compare these boundary conditions. Of course, the results of a computation depends only on the choice of the boundary (the rows in the table) and not on the form under which it is written (the columns in the table). It is straightforward to derive the 3D version of these correspondances (see table 2).

3.2 Practical implementation

To test these boundary conditions, we solve the two-dimensional compressible Euler equations with a Runge-Kutta integration. The boundary conditions are applied every sub-step. The calculations performed in the present study make use of the *COUPL* (Cerfacs and Oxford University Parallel Library) software library developed at CERFACS

Name	<i>temporal form</i>	<i>spatial form</i>
Thompson [24]	$\frac{\partial W^5}{\partial t} = 0$	$\frac{\partial W^5}{\partial n} = -\frac{u_{s1}}{u_n - c} \frac{\partial W^5}{\partial s_1} - \frac{u_{s2}}{u_n - c} \frac{\partial W^5}{\partial s_2} - \frac{c}{u_n - c} \frac{\partial W^2}{\partial s_1} - \frac{c}{u_n - c} \frac{\partial W^3}{\partial s_2}$
Poinsot [10]	$\frac{\partial W^5}{\partial t} = -u_{s1} \frac{\partial W^5}{\partial s_1} - u_{s2} \frac{\partial W^5}{\partial s_2} - c \frac{\partial W^2}{\partial s_1} - c \frac{\partial W^3}{\partial s_2}$	$\frac{\partial W^5}{\partial n} = 0$
Hirsh [11]	$\frac{\partial W^5}{\partial t} = -c \frac{\partial W^2}{\partial s_1} - c \frac{\partial W^3}{\partial s_2}$	$\frac{\partial W^5}{\partial n} = -\frac{u_{s1}}{(u_n - c)} \frac{\partial W^5}{\partial s_1} - \frac{u_{s2}}{(u_n - c)} \frac{\partial W^5}{\partial s_2}$
Giles [12]	$\frac{\partial W^5}{\partial t} = -u_n \frac{\partial W^2}{\partial s_1} - u_n \frac{\partial W^3}{\partial s_2} - u_{s1} \frac{\partial W^5}{\partial s_1} - u_{s2} \frac{\partial W^5}{\partial s_2}$	$\frac{\partial W^5}{\partial n} = \frac{\partial W^2}{\partial s_1} + \frac{\partial W^3}{\partial s_2}$

Table 2: Correspondance between the temporal and the spatial form for some non-reflecting boundary conditions. 3D case.

and Oxford University [27]. This library is used for a cell-vertex residual solver for unstructured and hybrid grids. Residuals are calculated element-wise, and distributed within each element to the nodes. For the application of the boundary conditions not based on the *full residual approach* (Thompson [24]) the contribution of the normal derivatives to the update of the boundary nodes are needed. This requires an extra step, since it is impossible to disentangle the normal contributions from the nodal update.

We start by calculating the element-wise gradients of \mathbf{V} , and equidistribute them to the nodes, to obtain a nodal approximation of $\vec{\nabla} \mathbf{V}$. Then, the normal derivative at the boundary is estimated as $\partial \mathbf{V} / \partial n = \vec{\nabla} \mathbf{V} \cdot \vec{n}$. The normal contribution is calculated as $-\Delta t \mathbf{E}_n \partial \mathbf{V} / \partial n$. Note that this approximation is quite different from the way the interior scheme is constructed. Consistency is much easier to ensure for a structured code.

3.3 The relation with the Riemann invariants

The Riemann invariants correspond to the integrated 1D characteristics variables, under the assumption of isentropic flow [11, 28]. They are:

$$R^1 = \frac{P}{\rho^\gamma}$$

$$\begin{aligned}
R^2 &= u_n + \frac{2c}{\gamma - 1} \\
R^3 &= u_n - \frac{2c}{\gamma - 1}
\end{aligned}
\tag{15}$$

These quantities are constant along the characteristics $dx/dt = u_n$, $dx/dt = u_n + c$ and $dx/dt = u_n - c$ respectively. To impose a non-reflecting outlet condition with $\vec{n} = (1, 0, 0)^t$, the variable at the boundary (subscript B) may be obtained as follows: R^3 is constant on a characteristic coming from outside the computational domain with state P^∞ , ρ^∞ and u^∞ . Thus the following relation holds:

$$u_B - \frac{2c_B}{\gamma - 1} = u^\infty - \frac{2c^\infty}{\gamma - 1} \tag{16}$$

Also, R^1 and R^2 are constant on outgoing characteristics so that

$$P_B / \overline{\rho_B^\gamma} = P_P / \overline{\rho_P^\gamma} \tag{17}$$

and

$$u_B + \frac{2c_B}{\gamma - 1} = u_P + \frac{2c_P}{\gamma - 1} \tag{18}$$

where the subscript P denotes predicted values due to the interior scheme. The relations (16)-(18) can be used to compute the variables at the boundary. A main difference between characteristic methods as given in table (1) and Riemann invariants approaches is that the latter technique imposes the *variables* on the boundary while the former impose the *variable variations*. Another difference is the assumption of isentropic flow which is not made in the treatments described in the previous subsections. An example of the effect of this hypothesis is given in the next section. In the following subsection, different simple academic test cases are considered to assess the efficiency of the different formulations.

3.4 Academic test cases

The tested formulations are designed as Riemann invariants, Giles [12], Poinot [10], Hirsh [11] and Thompson [24] (see table 1 for the definition of these conditions). Except otherwise stated, all the following computations are performed with a second-order centered scheme in space and a third order explicit Runge-Kutta time stepping. No artificial viscosity is used.

3.4.1 One-dimensional cases

A Gaussian perturbation of small amplitude is superimposed to the uniform density field and the other variables are initialized so as to

keep energy in only one mode of propagation, either the progressive acoustic one or the entropy one. The mean Mach number is set to 0.25 in both cases and the number of grid points is 201 (uniform mesh). Figures 1 and 2 show the convection of the acoustic perturbation through the evolution of density at different simulation times. The perturbation leaves the computation domain for $t = 0.5L/(U_0 + c)$, where L is the length of the domain and U_0 is the mean convection velocity. The bottom parts of the figures show that small numerical perturbations are created when the wave leaves the domain. These sawtooth instabilities have a non-physical negative group velocity of order $-U_0 - c$, in agreement with theoretical analysis [29]. The amplitude of the reflected perturbation is of order of 0.05% of the strength of the outgoing wave, showing that both the Thompson and the Riemann invariants approaches are efficient in this case. Similar results are obtained with the other characteristic treatments cited above. The results for the entropy wave are shown in figures 3 and 4. The characteristic approach produces the same type of result as for the acoustic wave, with the group velocity for the reflected numerical waves which is now of order $-U_0$. The use of the Riemann condition leads to the formation of a regressive acoustic wave ($U_0 - c$) when the entropic wave leaves the computation domain. The density perturbation associated with the reflected wave is even larger than the one related to the outgoing wave. This unacceptable behavior of the Riemann condition is a direct consequence of the isentropic flow assumption used to derive the invariants: this formulation should be used only for isentropic flows. Only characteristic treatments based on the variations of the primitive/characteristic vector will be considered in the following subsections.

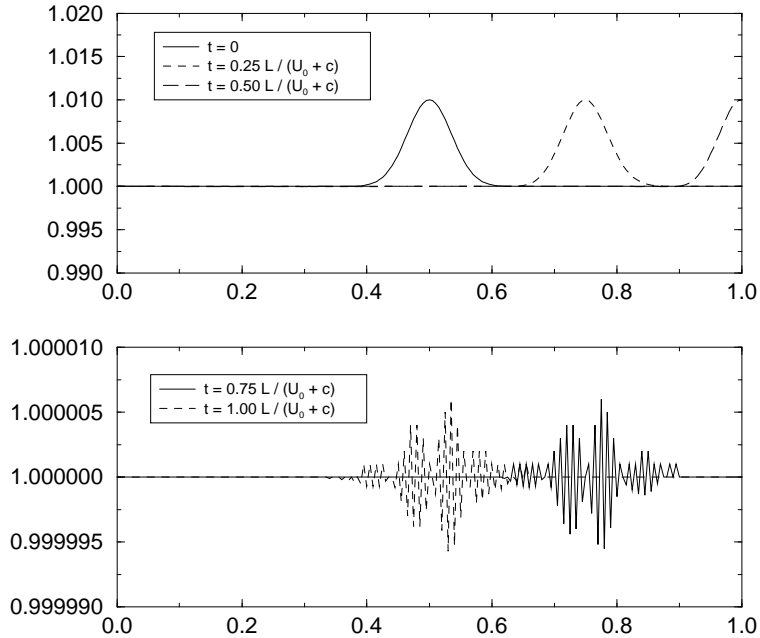


Figure 1: 1D acoustic wave. Spatial evolution of density before and after the acoustic wave leaves the domain using either of the conditions in table 1.

3.4.2 Two-dimensional shear layer

Consider the computation domain defined by $0 < x < 1$ and $0 < y < 1$. The initial condition is uniform for the density and the static pressure, zero for the velocity in the y -direction. For the streamwise velocity, we impose $u(x, y) = U_0(1.5 + \tanh(10(y - 0.5)))$ for $x = 0$, $u(y) = 0$ elsewhere. U_0 corresponds to 0.25 for the Mach number, so that the flow is subsonic everywhere. The Thompson (full residual) characteristic approach is used at the inlet to impose the velocity components and the temperature while a non-reflecting condition is tested at the outlet. The Poincot non-reflecting characteristic condition is used for both $y = 0$ and $y = 1$ to allow acoustic disturbances in the y -direction to leave the domain. The velocity profile is expected to propagate downstream during the computation. The steady solution is obviously $u(x, y) = u(0, y)$ for all x -values. Numerically, several convective times of propagation are simulated before the results are examined. Typical velocity profiles obtained with the Thompson formulation of the outlet

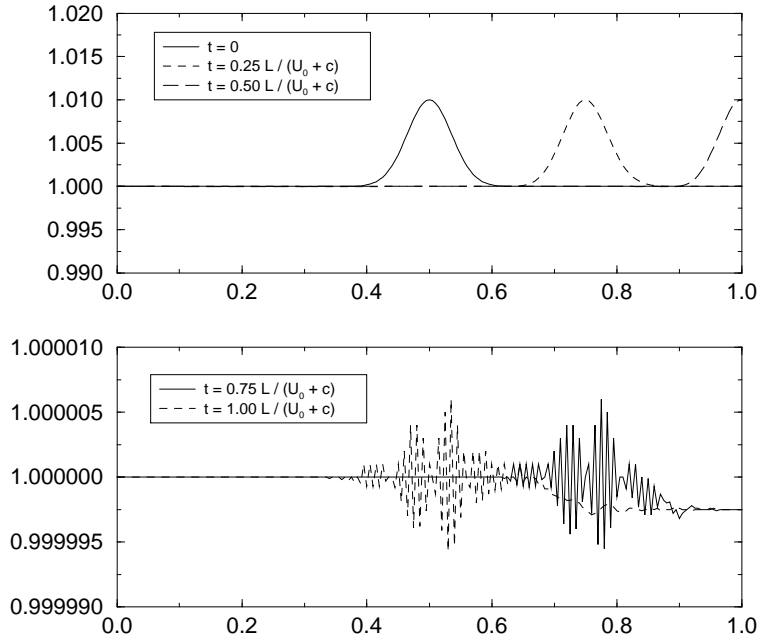


Figure 2: 1D acoustic wave. Spatial evolution of density before and after the acoustic wave leaves the domain using a non-reflecting condition based on the Riemann invariants.

boundary are shown in figure 5 . Clearly the outlet condition prevents the hyperbolic tangent profile from propagating along the x -direction. Instead, the u -velocity tends to be uniform near the exit. In fact this result is due to the formulation which, by imposing $\partial W_n^4 / \partial t = 0$, forces the temporal evolutions of the streamwise velocity and the pressure to remain nearly proportional (since $\partial W_n^4 = -\partial u + \frac{1}{\rho c} \partial P$) At the initial time, both quantities are uniform at the exit, so that their profiles keep the same shape during the computation if $1/\rho c$ does not depend on y . This feature of the boundary is well recovered by the computation (see figure 6) but is not compatible with the present physical configuration. Instead, the pressure profile should remain uniform and the u -profile should start from zero and tend to the imposed hyperbolic tangent profile at the inlet. The use of the Poinot's approach for the outlet leads to the correct behavior for the velocity profiles, as shown in figure 7. Indeed, the constraint on the ingoing acoustic wave is now written in terms of spatial gradients, so that the temporal evolutions of the pressure and the velocity at the exit are no more pro-

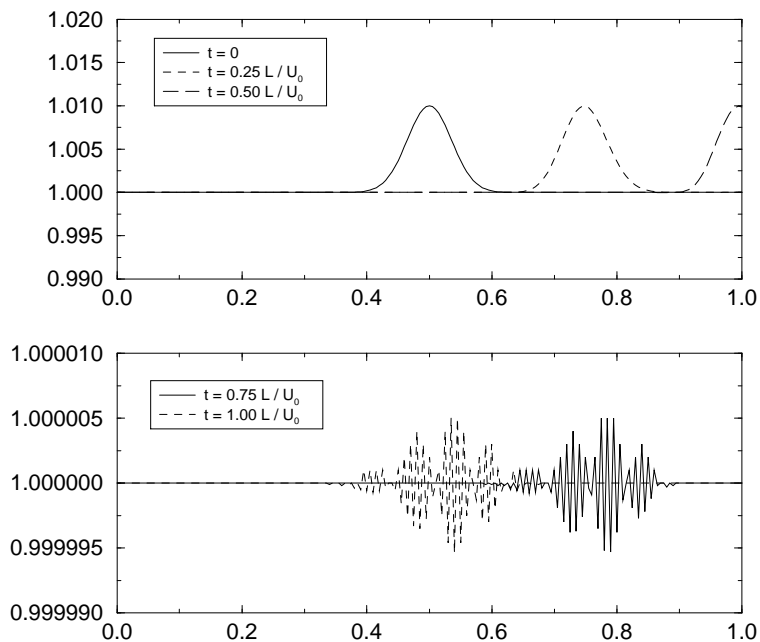


Figure 3: 1D entropy wave. Spatial evolution of density before and after the entropy wave leaves the domain using either of the conditions in table 1.

portional (see table 1). The correct behavior is also obtained for the other characteristic treatments cited above. However the computed physical time needed to reach the steady solution has been found to be greater for the Giles condition than for both the Poinot and the Hirsh formulations. By comparing these boundary conditions in table 1, it appears that three different terms appear in the right-hand-side of their *temporal forms*: $A = u_s \frac{\partial W^4}{\partial s}$, $B = c \frac{\partial W^2}{\partial s}$ and $C = u_n \frac{\partial W^2}{\partial s}$. At least one of these terms must be retained to reach the correct steady state. The Poinot's and the Hirsh's conditions leading to equivalent results, the A term above seems not critical for the present test case (this term is present in Poinot's formulation but not in Hirsh's, see table 1). Thus the B term is responsible for the success of the computations with those conditions. One observes also that the C term in the Giles condition is nothing but $\frac{u_n}{c} B$, smaller than B because the test case is subsonic. Thus the observed numerical result (longer relaxation time to the steady state with the Giles treatment) is consistent with the formal comparison of the different boundary conditions.

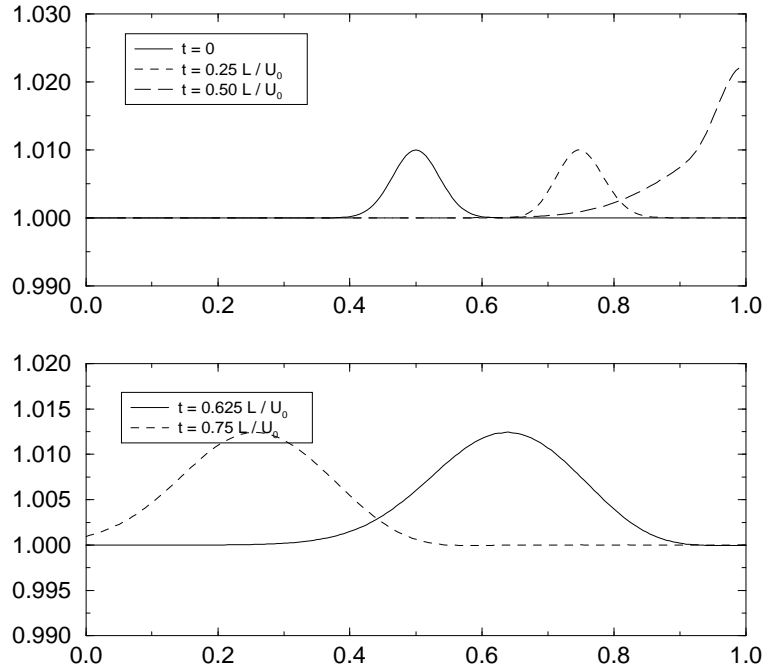


Figure 4: 1D entropy wave. Spatial evolution of density before and after the entropy wave leaves the domain using a non-reflecting condition based on the Riemann invariants.

3.4.3 Two-dimensional vortex

Consider the computation domain defined by $0 < x < 1$ and $0 < y < 1$ and the following stream function:

$$\psi(x, y, t = 0) = \psi_o e^{-\frac{((x-x_o)^2 + (y-y_o)^2)}{a^2}} \quad (19)$$

The corresponding velocity field $u = \frac{\partial \psi}{\partial y}$ and $v = -\frac{\partial \psi}{\partial x}$ defines a steady vortex centered at $x = x_o$ and $y = y_o$. ψ_o and a measure the strength and the size of the vortex respectively. The pressure field associated with this flow is $P = P_o - \rho \psi^2 / a^2$. To define the initial field, a uniform flow ($M = 0.25$) in the streamwise direction is superimposed to the previous vortex flow with $x_o = y_o = 0.5$. Two cases (A and B) have been computed. Table 3 gives the numerical values of the initial stream function ψ_o , the size of the vortex a and its strength, defined as $\omega_{max} a / U_0$. Case A corresponds to a weak vortex for which the induced velocity is only 1 % of the mean convection

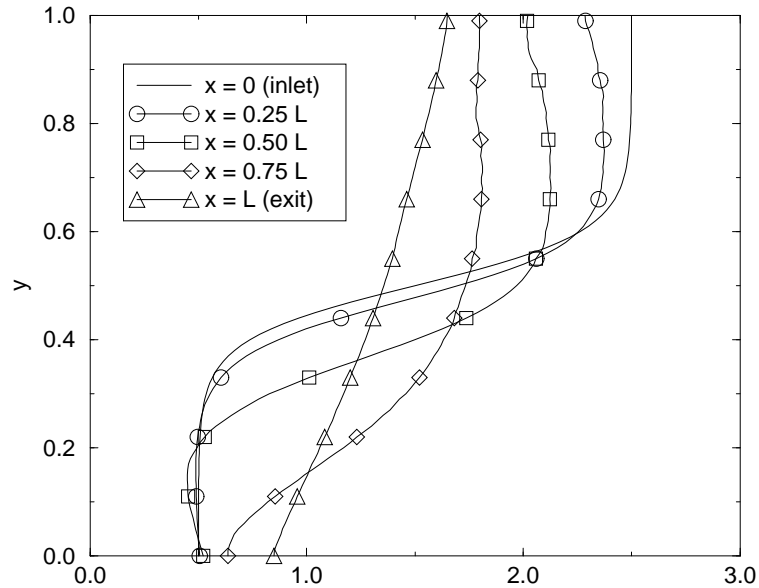


Figure 5: Two-dimensional shear layer. Velocity profiles at different abscissa for the Thompson's (full residual) non-reflecting outlet boundary condition.

Case	ψ_o	a	strength
A	0.0005	0.106	0.09
B	0.05	0.159	2.82

Table 3: Strength and size of the computed vortices.

velocity U_0 . The second case B stands for a strong vortex for which the induced velocity is 90 % of U_0 . Note that the absolute velocity is always positive for both cases so that the section $x = 1$ is always a subsonic outlet. The Poinot's non-reflecting characteristic condition is used for both $y = 0$ and $y = 1$ to allow the acoustic disturbances in the y -direction to leave the domain. It is also used for $x = 0$ while the tested non-reflecting boundary condition is used for $x = 1$. The vortex is convected downstream during the computation and leaves the domain at time $t = 0.5L/U_0$, where L is the length of the computation domain. With the Poinot's, Hirsh's and Giles's characteristic formulations for the outlet, the vortex leaves the domain and no vorticity perturbation is produced near the exit (not shown). Figures 8 and 9 show the root-mean-square value of both the vorticity (ω_{rms}) and the divergence

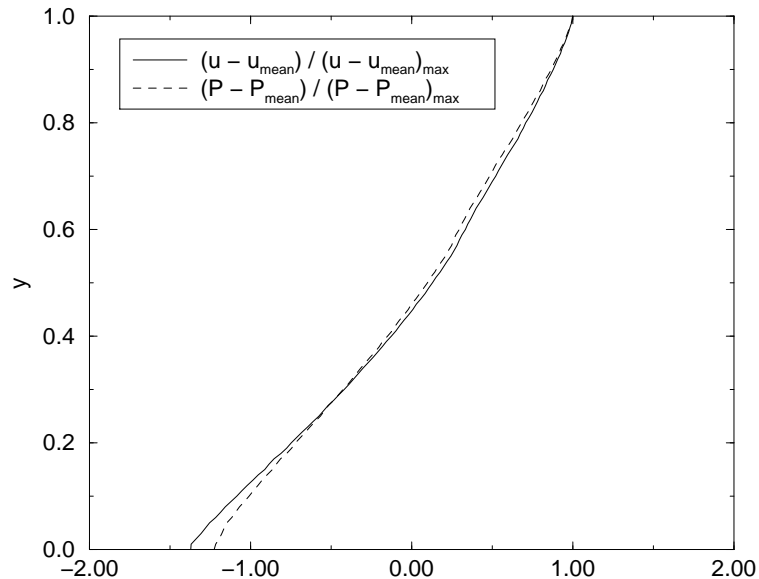


Figure 6: Two-dimensional shear layer. Comparison of the shape of the streamwise velocity and static pressure profiles at the exit plane. The shape of g is defined as $(g - g_{mean}) / (g - g_{mean})_{max}$, where g_{mean} is the mean value of g at the exit.

(div_{rms}) in the computation domain for Cases A and B. In the first stage of the simulation, both quantities show a plateau because the vortex is still in the domain and there is no dissipation. Around $t = 0.25L/U_0$, the vortex starts its interaction with the outlet boundary so that the divergence increases. At $t = 0.5L/U_0$, the center of vortex leaves the computation domain and the level of ω_{rms} sharply decreases. The acoustic perturbations propagate upstream and leave the domain through the different non-reflecting boundaries at the inlet and both the top and the bottom. After $t \simeq 1$, the level of divergence falls back to its initial value.

Figures 8 show the results for the Case A (weak vortex) with the outlet section treated with the Poinot [10] and the Giles [12] formulation respectively.¹ For both formulations, the computed time evolution of ω_{rms} compares well with the analytical one. This latter

¹The non-reflecting boundary condition given by Hirsh [11] produced results very similar to those obtained with the approach of Poinot so that the corresponding plots are not shown for clarity.

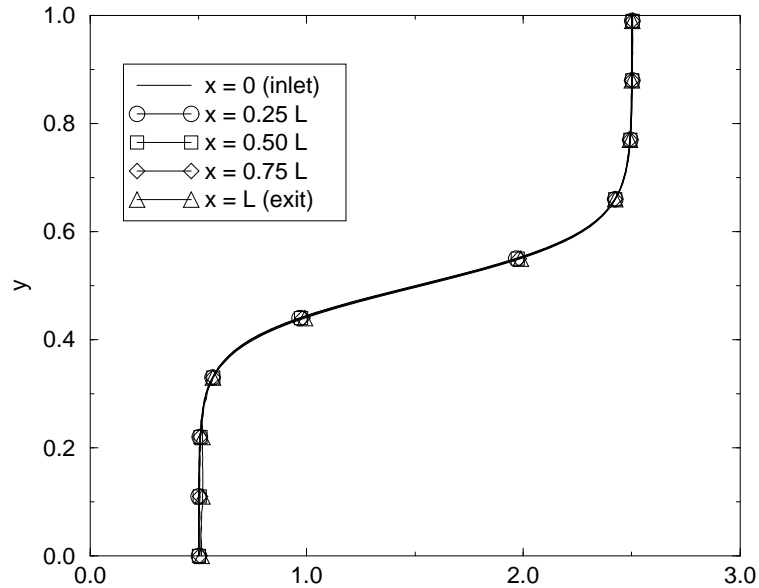


Figure 7: Two-dimensional shear layer. Velocity profiles at different abscissa for the Poinso's non-reflecting outlet boundary condition.

is the solution of the simple linear convection problem which is valid as long as the velocity induced by the vortex is small compared to the convection velocity. On the other hand, all boundary conditions produce an amount of dilatation which may be related to the amplitude of the reflected acoustic wave when the vortex leaves the domain [17]. A coefficient of acoustic reflection may be defined as the ratio of the maximum of divergence in the computation domain during the exit process to the maximum of vorticity in the incident vortex. It is much smaller for the Giles formulation than for the other one (4 %). Note that for the vortex strength and the spatial resolution considered in Case A, the amount of divergence produced by the Giles exit boundary is of the same order than the initial level of divergence which is related to the truncation error of the second-order spatial scheme used for the computations. As a consequence the reflexion coefficient for this case can hardly be measured except if the resolution is drastically increased. Instead, we preferred to increase the accuracy of the numerical method to check the behavior of the Giles condition in the linear range. Indeed, this condition is exact for the linearized Euler equations [12]. It is a second order condition so that the vorticity-acoustic reflexion

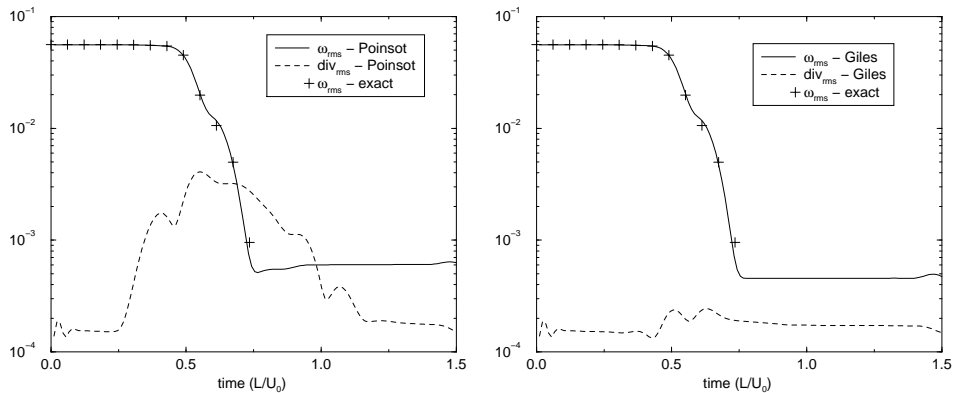


Figure 8: 2D vortex. Time evolutions of the rms of vorticity and divergence during the exit of a linear (weak) vortex through a non-reflecting subsonic outlet condition. Case A - Treatment of Poincot (left) and Giles (right).

coefficient should go to zero as the strength of the vortex does. On the other hand, the first order Poincot condition should produce a nearly constant reflexion coefficient when the scheme accuracy changes. These features have been well recovered in the present study (see figure 10) by using a sixth-order compact scheme and a third order Runge-Kutta formulation for the time stepping.

Figures 9 correspond to case B. Even for the non-linear vortex, the decrease of vorticity in the computation domain is well reproduced by both boundary treatments. Note that the 'exact' solution in these figures correspond to a simulation with a domain of length 2, the root-mean-square of vorticity being computed over the first half of it. In terms of reflected acoustic wave, the difference between the two boundary treatments decreases when the strength of the vortex increases, as suggested by figure 10. For case B, both conditions lead to the same order of reflexion coefficient (around 4 % for both). This is due to non-linear effects which are not properly accounted for, independently of the boundary formulation. A way to overcome this difficulty is to insert a buffer region before the exit section, so as to make the perturbation linear before it interacts with the boundary [17].

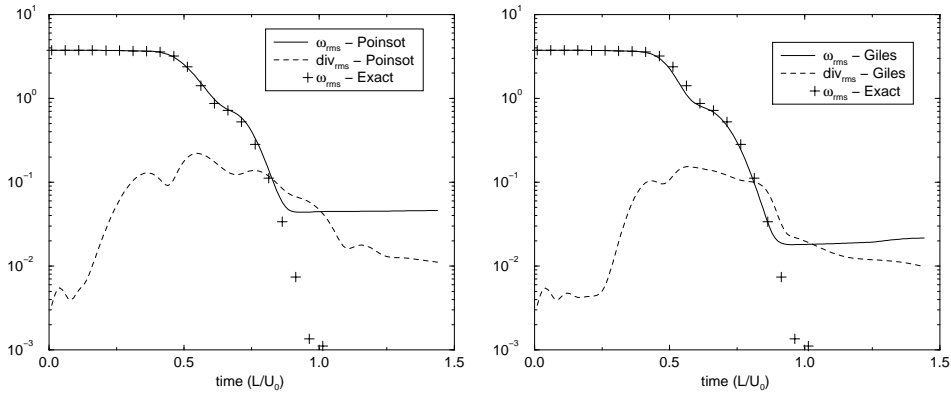


Figure 9: 2D vortex. Time evolutions of the rms of vorticity and divergence during the exit of a non-linear (strong) vortex through a non-reflecting subsonic outlet condition. Case B - Treatment of Poinot (left) and Giles (right).

3.5 Lack of reference

Using non-reflecting boundary conditions for Navier-Stokes equations is very appealing but requires some caution since building a perfectly non-reflecting condition might not lead to a well-posed problem. Suppose that we want to compute a free shear layer by using the inlet boundary conditions described in the previous section, i.e., by imposing the inlet velocities and the temperature. If we build 'perfectly non-reflecting' boundary conditions for the three other sides of our domain, we should wonder how the flow will determine what the mean pressure will be. Physically, this information is conveyed by waves reflecting on regions far from the computation domain where some static pressure p_∞ is specified and propagating back from the outside of the domain to the inside through the boundaries. With perfect boundary condition this information will never be fed back into the computation and the problem might be ill-posed. Corrections may be added to the treatment of boundary conditions to make them only partially non-reflecting. A way to do this for a subsonic outlet is to prescribe

$$\frac{\partial W^5}{\partial t} + K(p - p_\infty) = 0 \quad (20)$$

where the term $K(p - p_\infty)$ is written as $K = \sigma'(1 - M^2)c/L$ where c is the speed of sound, L a characteristic size of the domain and M the characteristic Mach number. By studying analytically the behavior of Eq. (20) for a linearized constant coefficient one-dimensional system of equations [15], it is possible to show that an optimal value for σ'

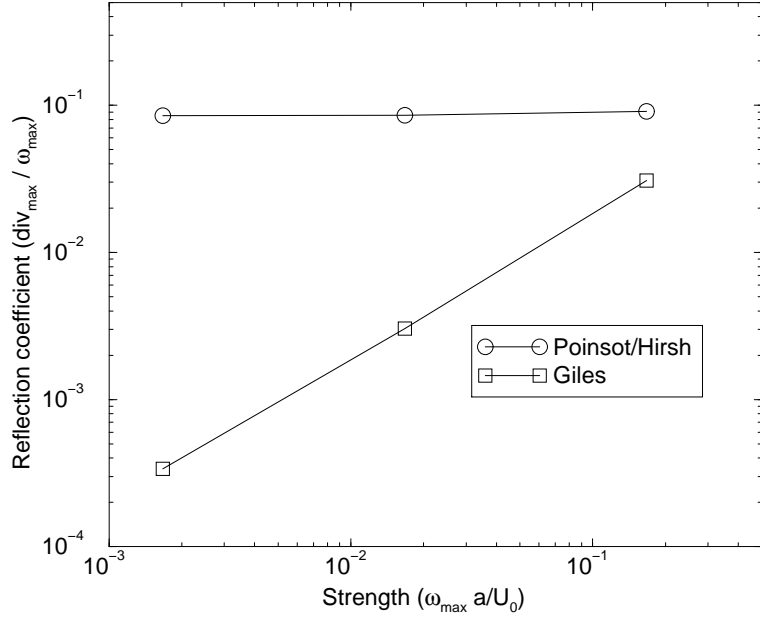


Figure 10: 2D vortex. Coefficient of acoustic reflection as a function of the amplitude of the incident vortex. Comparison between a first order (Poinsot, Hirsh) and a second order (Giles) condition in the linear range. Results from a code based on a sixth-order compact scheme.

is 0.27. However, some tests in [15] show that a value of 0.58 provide the best results in practice. For practical applications we have found that the results do not depend drastically on K as soon as it is large enough to prevent the mean pressure to drift.

The same idea may be useful to weakly prescribe some quantity (the velocity, say) at an inlet boundary. The exact way of doing it would be to compute the incoming acoustic wave as $\frac{\partial W_n^4}{\partial t} = \frac{\partial W_n^5}{\partial t}$ which would induce $\delta u_n = 0$ from Eq. (7). Instead one can impose $\frac{\partial W_n^4}{\partial t} = -K_u(u_n - u_{ref})$ where u_{ref} is a reference velocity profile. This condition would act as non-reflecting if u_n is close to u_{ref} but would prevent u_n from being too different from the arbitrary reference.

4 Generalization to the Navier-Stokes Equations

The concept of 'characteristic lines' may be questionable for the Navier-Stokes equations and it seems that no general theory is available yet for prescribing fully consistent boundary conditions in the viscous case. The method presented here is very close to the Navier-Stokes Characteristic Boundary Conditions –NSCBC [10]. This method is valid for Navier-Stokes and Euler equations and relaxes smoothly from one to the other when the viscosity goes to zero. The number of conditions specified for the viscous case is that obtained by theoretical analysis of well-posedness [30].

Complete Navier-Stokes Boundary Conditions are obtained by using Euler inviscid Boundary Conditions and supplementing them with additional viscous conditions. These additional conditions must have a negligible effect when the viscosity goes to zero and their implementation is not done at the same level as the inviscid conditions. In the present procedure, we consider that the inviscid conditions are applied by using the *normal* approach where the wave amplitude are defined on the variation $\delta\mathbf{V}_w^P = -\Delta t\mathcal{R}_n$ of the primitive variables (see 2). The viscous conditions are applied only during the final update of the boundary point (see 2):

$$\mathbf{V}^{n+1} = \mathbf{V}^n + \delta\mathbf{V}^U + \delta\mathbf{V}_w^C = \mathbf{V}^n + \delta\mathbf{V}^U + \delta\mathbf{V}^{in,C} + \delta\mathbf{V}^{out}$$

by specifying those viscous and diffusion terms in $\delta\mathbf{V}^U$.

We have not indicated yet how to choose the viscous conditions. The compatibility of inviscid conditions with viscous conditions is not automatically ensured. Most Navier-Stokes codes actually use physical Boundary Conditions derived for the Euler equations. In particular, the number of physical conditions imposed on a given boundary is often chosen as if the flow were inviscid by arguing that the boundaries are far enough from the regions where viscous effects are important. As a consequence, only inviscid conditions are applied and no viscous conditions are introduced.

In the NSCBC method, the number and the choices of physical Boundary Conditions (inviscid and viscous) were guided using the theoretical studies of Strikwerda [30] and Oliger and Sundström [31]. The most common subsonic inflow and outflow conditions are considered in table 4 which summarizes the different physical conditions used in the NSCBC method for a three-dimensional flow. The case of Euler equations is also displayed in the left column of each table to allow comparison with Navier-Stokes. In general, it is fair to say that only small effects are caused by these viscous conditions for inlets (this is

BOUNDARY TYPE	EULER	NAVIER-STOKES
Isothermal Inlet	u, v, w, T imposed	nothing
Non-Reflecting Inlet	$\delta W_n^j = 0, j = 1, 4$	$\frac{\partial \tau_{nn}}{\partial x_n} = 0$
Isobaric Outlet	P imposed	$\frac{\partial \tau_{nj}}{\partial x_n} = 0, j \neq n; \frac{\partial q_n}{\partial x_n} = 0$
Non-Reflecting Outlet	$\delta W_n^5 = 0$	$\frac{\partial \tau_{nj}}{\partial x_n} = 0, j \neq n; \frac{\partial q_n}{\partial x_n} = 0$
Isothermal Wall	$u, v, w = 0; T$ imposed	nothing
Adiabatic Wall	$u, v, w = 0$	$q_n = 0$

Table 4: Some physical Boundary Conditions for 3D Flows for Euler and Navier-Stokes Equations.

not true for outlets).

5 Examples

This section presents two examples to illustrate the drastic effect of the boundary conditions in unsteady computations. The first case is the flow over a ramp which acts as an artificial resonator. The flow over a shallow cavity is then considered.

5.1 Detached flow over a ramp

This configuration has been considered in [32, 33] to study the effect of an active control technique applied to a detached boundary layer. The principle of the numerical setup is given in figure 11. A laminar boundary layer is imposed at the inlet and develops until the geometrical discontinuity. If the Reynolds number is sufficiently large, the flow detaches due to the adverse pressure gradient and may become unstable. A vortex shedding phenomenon is observed if the Reynolds number further increases. Physically, the Strouhal number based on the momentum thickness is fixed because the vortex shedding phenomenon is related to the Kelvin-Helmoltz instability in the shear layer which develops near the corner. The vortices generated due to the hydrodynamic instability are convected and eventually dissipated far downstream of the ramp discontinuity. Numerically, the vortical structure are not dissipated before they leave the computational domain and they interact with a non-reflecting outlet boundary condition (see figure 11). This interaction generates some noise as shown in section 3.4.3. The pressure perturbation propagates upstream and can trigger a new instability within the shear layer which develops near the corner. With such a scenario, the frequency f for the vortex shedding is related to (non-physical) length of the computational domain L by the

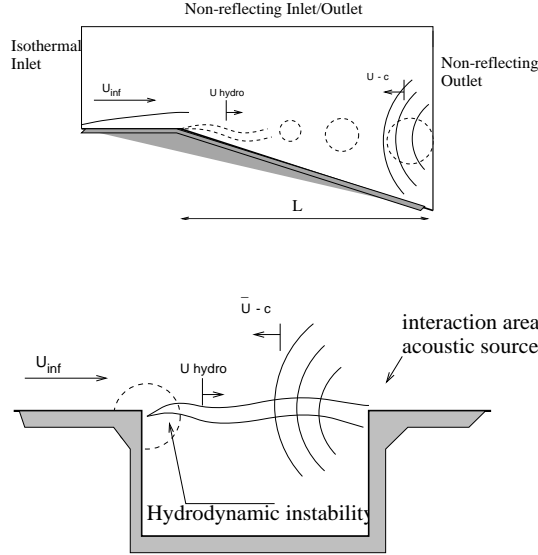


Figure 11: Computational domain and feedback coupling for the flow over a ramp (top), over a cavity (bottom).

relation:

$$\frac{n}{f} = \frac{L}{U_c} + \frac{L}{c - U_c} \quad (21)$$

where U_c is the mean convection velocity along the vortices path, n is the number of structures present at the same time in the domain and c is the speed of sound. The tests performed in [33] show that the frequency of the vortex shedding scales on the domain length L , as suggested by the previous relation. The same dependence was observed for all non-reflecting boundary condition as well as for a pressure imposed outlet. Note that the feedback mechanism is physical and expected for this latter boundary condition. It seems that no non-reflecting boundary condition exists which keeps the noise generated when a vortex leaves the domain small enough to prevent the feedback coupling to occur. The only way to proceed seems to artificially damp the vortical structure before it leaves the domain. One way is to introduce a viscous buffer layer before the exit [17] or to increase the domain size as shown in the next subsection.

5.2 Flow over a cavity

Another interesting class of flow/acoustic coupling is observed in cases where a feedback phenomenon is expected to take place due to a vortex-

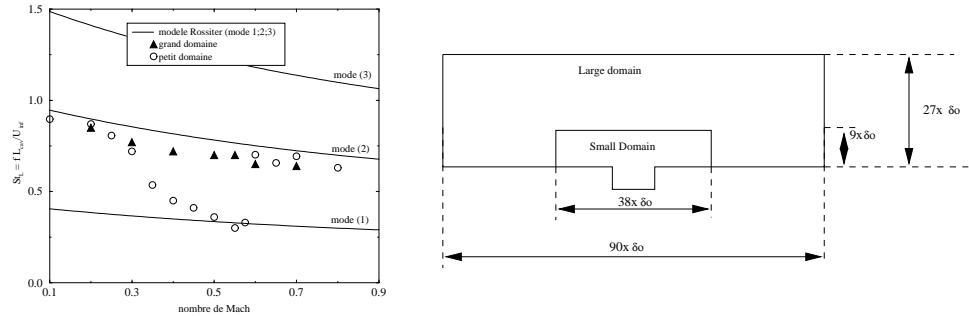


Figure 12: **Left:** Frequency of the instability of the flow over a cavity as a function of the Mach number. For the small domain, the spurious acoustic reflexion at the exit modify the global feedback phenomenon while the Rossiter branch $n = 2$ is well reproduced for the larger domain. **Right:** Computational domains for the flow over a cavity.

wall interaction as discussed in [5]. In the case of a flow over a cavity for example, the hydrodynamic instability which takes place in the shear layer close to the upstream corner develops and is convected downstream by the mean flow (see figure 11). The vortex induced by this instability interacts with the downstream corner and the noise created by the interaction propagates upstream. The pressure wave triggers a new hydrodynamic instability and the shedding frequency is given by Eq. (21) with L the length of the cavity. A formula of this form was first proposed by Rossiter [34] and was found in good agreement with the experimental data. Note that for a given mode (n fixed), the frequency decreases slightly when the Mach number of the outer flow increases. This behaviour is not reproduced numerically when the computational domain is "small" but the frequency reduction is well reproduced for a larger domain (see figure 12). A close examination of the solutions shows that a vortex is torn during its interaction with the downstream corner. The lower part of the vortex feeds the recirculation region within the cavity while the upper part is convected by the boundary layer downstream of the cavity. In the small domain case, the secondary vortex is not damped before it leaves the computational domain and the spurious noise can modify the physical feedback for certain flow conditions. This problem is present for all the boundary treatments considered previously (Poinsot, Hirsh, Giles) because the vorticity-dilatation reflexion coefficient is similar for these conditions in the case of strong vortices (see figure 10). In the case of a larger domain, the vortices are damped before the exit and no spurious reflexion can modify the unsteady solution. More details about this configura-

tion can be found in [35, 36, 37].

6 Conclusion

The general framework for characteristic-based boundary conditions for Euler equations is recalled. The particular case of non-reflecting outlet is considered to show that several previous proposals can be written within the same framework. Both analytical and numerical comparisons are performed. The Riemann invariant approach produces a very large entropy-acoustic reflexion coefficient, even for the simplest 1D inviscid case. Concerning the boundary treatments based on the variations of the variables, it is shown that the considered formulations can be written in two equivalent forms, namely the *temporal* form and the *spatial* form. In the former one the boundary conditions are expressed in terms of time derivative of the ingoing characteristic variable. This particular form is used to analyse some of the errors observed during the computations. Noticeably, the *full residual* formulation [9] is shown unable to forget to initial state at the boundary section, even after the characteristic time of the problem is computed several times. As concerns the vorticity-acoustic reflexion coefficient, the second order Giles formulation [12] is found more accurate than other first order boundary conditions (Poinsot [10], Hirsh [11]) in the case of weak vortices. However a very accurate method is needed to measure the gain of this formulation, and none of the tested treatments gives fully satisfactory results for stronger vortices. The generalization to Navier-Stokes equations proposed in [10] is finally briefly discussed and computations of aeroacoustic instabilities over a ramp and a cavity are shown in order to demonstrate the sensitivity of the results on the boundary treatment.

References

- [1] H.O. Kreiss. Initial boundary value problems for hyperbolic systems. *Commun. Pure Appl. Math.*, 23:277, 1970.
- [2] B. Engquist and A. Majda. Absorbing boundary conditions for the numerical simulation of waves. *Mathematics of Computation*, 31(139):629–651, 1977.
- [3] R.L. Higdon. Initial-boundary value problems for linear hyperbolic systems. *SIAM Rev.*, 28:177–217, 1986.
- [4] B. Gustafsson and A. Sundstrom. Incompletely parabolic problems in fluid dynamics. *SIAM J. Appl. Math.*, 35(2):343, 1978.

- [5] D. Rockwell and E. Naudascher. Self-sustained oscillations of impinging free shear layers. *Ann. Rev. Fluid Mech.*, 11:67–94, 1979.
- [6] J.C. Buell and P. Huerre. Inflow/outflow boundary conditions and global dynamics of spatial mixing layers. *Center for Turbulence Research, CTR Annual Research Briefs*, pages 19–27, 1988.
- [7] C. Tam and L. Auriault. Time-domain impedance boundary conditions for computational aeroacoustics. *AIAA Journal*, 34(5):917–923, 1996.
- [8] S. Chakravarthy. Euler equations - implicit scheme and boundary condition. *AIAA Journal*, 21:699–706, 1983.
- [9] K.W. Thompson. Time dependant boundary conditions for hyperbolic systems. *Journal of Computational Physics*, 68:1–24, 1987.
- [10] T.J. Poinso and S.K. Lele. Boundary conditions for direct simulations of compressible viscous flows. *Journal of Computational Physics*, 101:104–129, 1991.
- [11] C. Hirsh. *Numerical computation of internal and external flow.*, volume 2. J. Wiley and Sons, New York, 1990.
- [12] M. Giles. Non-reflecting boundary conditions for euler equation calculation. *AIAA Journal*, 28(12):2050–2058, 1990.
- [13] M. Hayder and E. Turkel. Nonreflecting boundary conditions for jet flow computations. *AIAA Journal*, 33(12):2264–2270, 1995.
- [14] H. Atkins and J. Casper. Nonreflective boundary conditions for high-order methods. *AIAA Journal*, 32(3):512–518, 1994.
- [15] D. Rudy and J. Strikwerda. A nonreflecting outflow boundary condition for subsonic navier-stokes equations. *Journal of Computational Physics*, 36:55–70, 1980.
- [16] D. Givoli. Non-reflecting boundary conditions. *Journal of Computational Physics*, 94:1–29, 1991.
- [17] T. Colonius, S.K. Lele, and P. Moin. Boundary conditions for direct computation of aerodynamic sound generation. *AIAA Journal*, 31(9):1574–1582, 1993.
- [18] S. Ta’asan and D. Nark. An absorbing buffer zone technique for acoustic wave propagation. *AIAA Paper 95-0146*, 1995.
- [19] J. Freund. Proposed inflow/outflow boundary condition for direct computation of aerodynamic sound. *AIAA Journal*, 35(4):740–742, 1997.

- [20] K. Mazaheri and P.L. Roe. Numerical wave propagation and steady-state solutions: Soft wall and outer boundary conditions. *AIAA Journal*, 35(6):965–975, 1997.
- [21] M.D. Griffin and J.D. Anderson. On the application of boundary conditions to time dependent computations for quasi-one dimensional fluid flows. *Computers and Fluids*, 5:127–137, 1977.
- [22] D. Gottlieb and E. Turkel. Boundary conditions for multistep finite difference methods for time-dependent equations. *Journal of Computational Physics*, 26:181–196, 1978.
- [23] H.C. Yee, R.M. Beam, and R.F. Warming. Boundary approximation for implicit schemes for one-dimensional inviscid equations of gas dynamics. *AIAA Journal*, 20:1203–1211, 1982.
- [24] K.W. Thompson. Time dependant boundary conditions for hyperbolic systems, ii. *Journal of Computational Physics*, 89:439–461, 1990.
- [25] F. Nicoud. Defining wave amplitude in characteristic boundary conditions. *Journal of Computational Physics*, 149(2):418–422, 1999.
- [26] M. Hayder and E. Turkel. High order accurate solutions of viscous problems. *AIAA Paper 93-3074*, 1993.
- [27] M. Rudgyard, T. Schönfeld, R. Struijs, and G. Audemar. A modular approach for computational fluid dynamics. *Proceedings of the 2nd ECCOMAS-Conference, Stuttgart*, 1994. Also exists as CERFACS Technical Report TR/CFD/95/07.
- [28] J.D. Anderson. Modern compressible flow (with historical perspective). *McGraw-Hill, New-York*, 1982.
- [29] R. Vichnevetsky and J.B. Bowles. Fourier analysis of numerical approximations of hyperbolic equations. *SIAM Philadelphia*, 1982.
- [30] J.C. Strikwerda. *Commun. pure appl. math.* 30, 797, 1977.
- [31] J. Olinger and A. Sundström. *SIAM J. Appl. Math.*, 35:419, 1978.
- [32] G. Hernandez, T. Schönfeld, N. Mangiavacchi, and F. Nicoud. Numerical active control of two-dimensional boudary layer separation. *AIAA Paper 96-2142*, 1996.
- [33] G. Hernandez, F. Nicoud, and T. Poinso. titre a voir avec greg. *AIAA Journal*, submitted, 1998.
- [34] J.E. Rossiter. Wind tunnel experiments in the flow over regular cavities at subsonic and transonic speeds. *R and M*, page 3438, 1966.

- [35] T. Kestens and F. Nicoud. Calcul d'un écoulement au dessus d'une cavité rectangulaire. *Colloque Association Universitaire de Mécanique, 1-5 Septembre 1997, Poitiers, 1997.*
- [36] T. Kestens and F. Nicoud. Active control of an unsteady flow over a rectangular cavity. *AIAA Paper 98-2348, 1998.*
- [37] T. Kestens. Etude numérique du contrôle adaptatif multivoies des instabilités aéroacoustiques des cavités. *Thesis, Institut National Polytechnique de Toulouse, 1999.*